A WAVES-IN-ICE MODEL WITH A FLOE-BREAKING PARAMETERISATION

T. D. Williams[1], **L G. Bennetts**[2] **and V. A. Squire**[3]

[1]**Nansen Environment & Remote Sensing Centre, Bergen, Norway (timothy.williams@nersc.no)**

[2]**University of Adelaide, Adelaide, Australia (luke.bennetts@adelaide.edu.au)**

[3]**University of Otago, Dunedin, New Zealand (vernon.squire@otago.ac.nz)**

Introduction

Access to the ice-covered regions of the ocean is increasing due to the impact of climate change, and demand for more accurate forecasting of the conditions in these areas is therefore rising. The presence of waves, either propagating from the open ocean or generated by local fetch, presents a hazard to offshore activities, as it significantly increases the dynamics of the ice cover. However, contemporary wave models (e.g. WAM, WAVEWATCH III) are unable to operate in the ice-covered regions of the ocean, and sea ice models do not account for the effects of waves. A project (WIFAR: Waves in ice forecasting for Arctic operators) with the objective to create the first waves-in-ice component for a coupled ice/ocean forecasting model commenced in 2010, and a one-dimensional prototype for the coupled wave-ice component of the model was presented by *Dumont et al.* (2011). Here we report further developments of this waves-in-ice model (WIM) made during the project, and highlight some of the issues that need to be considered in order make the model fully operational.

Sea ice response to atmospheric or oceanic forcing depends on its structure. In particular, the part of the ice cover adjacent to the open ocean, known as the marginal ice zone (MIZ), behaves very differently to the consolidated pack ice it encloses, as it is comprised of relatively small ice floes, separated by open water. This is a direct consequence of strains imposed on the ice cover by passing waves. However, wave energy also dissipates with distance into the ice-covered ocean, so the net result is that floe sizes increase away from the ice edge. Far enough away from the edge, the waves are no longer strong enough to cause fracture and the ice cover becomes quasi-continuous, signalling the transition from the MIZ to the inner pack ice.

The WIM under construction incorporates the coupled effects of floe breaking induced by waves and the attenuation of wave energy due to the presence of the ice cover. The ice cover can therefore be divided into at least two regions; the MIZ and quasi-continuous ice. Appropriate rheological models are then applied to describe the large scale dynamics of the ice cover. The wave-ice component is being incorporated into a high resolution ($\sim$3.5 km) operational model (a version of HYCOM: hybrid coordinate ocean model) in the Fram Strait between Greenland and Svalbard. The component couples an outer wave model that provides the wave forcing, and a sea-ice model that provides ice conditions such as average thickness and surface concentration.

The new wave-ice parameterisations are also being tested in simplified one-dimensional settings (as done by *Dumont et al.*, 2011), prior to integration into the full model, and a selection of results are shown here. Preliminary results for the extension to the two-dimensional model are given at the end of the abstract.

The waves-in-ice model

The WIM that will be discussed in this work functions on small to medium scales. At the medium scale, waves are advected from the open ocean into the ice-covered ocean and are attenuated. The latter is primarily a product of small scale scattering events at the edges of individual floes. The bridge between the small-to-medium and large scales is the floe size distribution (FSD) which determines which rheology to use at a particular point in time and space. It also has a significant effect on the large scale dynamics and thermodynamics of the ice cover, as, for example, smaller floes are more prone to lateral melting. Wave-induced ice breaking alters the FSD, lowering the mean floe length, which consequently increases the amount of wave attenuation, thus constructing a feedback loop.

The wave information is contained in the spectral density function $S(\omega, \theta, \mathbf{x}_{ij}, t_n)$, which depends on radial frequency $\omega = 2\pi/T$ (T is the wave period), wave direction θ, position and time (both discretised). By convention, θ is the direction that the waves are coming *from* and is measured clockwise from north. Integrals of this quantity, with respect to frequency and direction, give statistical information about the expected sizes of waves and induced strains, and their regularity (*WMO*, 1998, §1.3.8). If we define $\langle w^2 \rangle$ and $\langle \varepsilon^2 \rangle$ as the mean square displacement of the ice and strain in the ice (respectively), and N_{W} as the expected number of waves in a given time interval $\Delta t = t_n - t_{n-1}$, then

$$\langle w^2(\mathbf{x}_{ij}, t_n) \rangle = m_0(\mathbf{x}_{ij}, t_n), \quad N_{\mathrm{W}}(\mathbf{x}_{ij}, t_n) = \frac{\Delta t}{2\pi} \sqrt{\frac{m_2(\mathbf{x}_{ij}, t_n)}{m_0(\mathbf{x}_{ij}, t_n)}} \tag{1a}$$

$$m_r(\mathbf{x}_{ij}, t) = \int_0^\infty \int_0^{2\pi} S(\omega, \theta, \mathbf{x}_{ij}, t_n) \left(\frac{k_{ij}}{k} \right)^2 \omega^r \mathrm{d}\theta \mathrm{d}\omega, \tag{1b}$$

$$\langle \varepsilon^2(\mathbf{x}_{ij}, t_n) \rangle = \int_0^\infty \int_0^{2\pi} S(\omega, \theta, \mathbf{x}_{ij}, t_n) \left(\frac{k_{ij}}{k} \times \frac{k_{ij}^2 h_{ij}}{2} \right)^2 \mathrm{d}\theta \mathrm{d}\omega. \tag{1c}$$

Here $k = \omega^2/g$ is the open-water wavenumber in water of infinite depth, g is the gravitational acceleration, h_{ij} is the ice thickness and k_{ij} is the ice-coupled wavenumber. We characterise the wave spectrum by the peak period, T_{M}, the significant wave height $H_s(\mathbf{x}_{ij}, t_n) = 4\langle w^2(\mathbf{x}_{ij}, t_n) \rangle^{1/2}$, and mean wave direction $\langle \theta \rangle$. In the full model this information is provided by

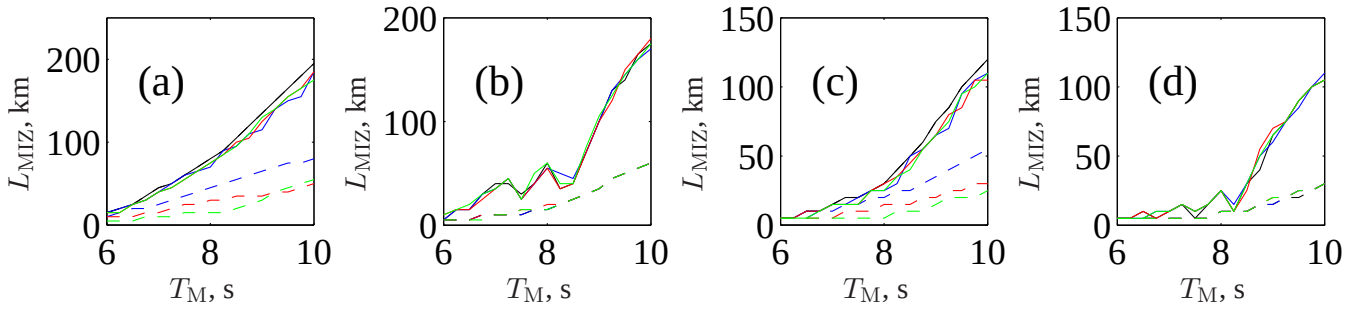

Figure 1: The effect of changing the AAS (Advection-Attenuation Scheme) on L_{MIZ}. The concentration is set to a uniform 0.75, and $H_s = 3\,\mathrm{m}$. The ice thickness is 2 m in figures (a-b), and 3 m in figures (c-d). The solid lines correspond to AAS 2 and the dashed lines to AAS 1. In (a, c), the time step is set to 260 s and the wave speed is set to $\mathcal{C}\Delta x/\Delta t$ for all wave frequencies, while in (b, d), the same time step is used, but dispersive effects are included by setting the wave speeds to $\beta g/(2\omega) \times \mathcal{C}\Delta x/\Delta t$, where $\beta = (4\pi\,\mathrm{s}^{-1})/(25g)$. In all plots, $\mathcal{C} = 1$ (black curves), 0.9 (blue curves), 0.8 (red curves) and 0.7 (green curves). Note that the two AASs agree when $\mathcal{C} = 1$.

an external wave model (WAM). We summarise the information contained in the strain spectrum by the significant strain amplitude $E_s(\mathbf{x}_{ij}, t_n) = 2\langle\varepsilon^2(\mathbf{x}_{ij}, t_n)\rangle^{1/2}$, which we shall use later to determine the probability of breaking occurring. In the open ocean we assume S is initially a Bretschneider spectrum multiplied by a simple directional spreading function:

$$S(\omega, \theta, \mathbf{x}_{ij}, t_0) = \frac{1.25 H_{\mathrm{s}}^2 T^5}{8\pi T_{\mathrm{M}}^4} \mathrm{e}^{-1.25(T/T_{\mathrm{M}})^4} \times G\big(\theta - \langle\theta\rangle\big), \tag{2a}$$

$$G(\theta) = \begin{cases} \frac{2}{\pi}\cos^2\theta & \text{if } |\theta| \le \frac{\pi}{2}, \\ 0 & \text{if } \frac{\pi}{2} < |\theta| < \pi. \end{cases} \tag{2b}$$

Having prescribed our initial conditions, we can now summarise the procedure the WIM goes through each time step.

1. *Advection.* Let $\big[\boldsymbol{S}_n(\omega)\big]_{ij} = S(\omega, \theta, \mathbf{x}_{ij}, t_n)$. We already have initial conditions from (2), and then we have an advection operator $\boldsymbol{\mathcal{A}}$ that changes $\boldsymbol{S}_{n-1}$ to an intermediary $\tilde{\boldsymbol{S}}_n = \boldsymbol{\mathcal{A}}(\boldsymbol{S}_{n-1}, \mathbf{a})$, where $[\mathbf{a}(\omega)]_{ij} = a_{ij}(\omega) = \mathrm{d}\omega/\mathrm{d}k_{ij}$ is the group velocity. (In open water, $a_{ij}(\omega) = a(\omega) = g/(2\omega)$.) This provides the unattenuated wave spectrum.

2. *Attenuation.* Let D_{ij}^{M} and $\langle D_{ij}\rangle$ be the maximum and mean floe sizes in a given grid cell. We assume the FSD is either the same or is a similar power law distribution as used by *Dumont et al.* (2011), which lets us determine $\langle D_{ij}\rangle$ from D_{ij}^{M}. We then look up the pre-calculated non-dimensional attenuation coefficients μ_{ij}^s and μ_{ij}^d, using the model of *Bennetts & Squire* (2012). The former coefficient is calculated using the 'average' scattering from single ice edges, while the latter provides additional damping for long waves using an empirical fit to the most reliable experimental data available at present (*Squire and Moore*, 1980). We then add the two effects together to get $\mu_{ij} = \mu_{ij}^s + \mu_{ij}^d$ and calculate $\boldsymbol{S}_n$ from

$$S(\omega, \theta, \mathbf{x}_{ij}, t_n) = \tilde{S}(\omega, \theta, \mathbf{x}_{ij}, t_n) \times \exp\left(\frac{-\mu_{ij} c_{ij}}{\langle D_{ij}\rangle}\right).$$

3. *Probability of breaking.* Wave *amplitudes* (denoted A, and defined as half the distance from a peak to the following trough) are generally assumed to follow a Rayleigh distribution (*WMO*, 1998, §1.3.6–1.3.8), so we will also assume that the strain *amplitudes* (denoted E, and defined analogously to A) follow one too. That is, for prescribed A_c and ε_c,

$$\mathbb{P}(A > A_c) = \exp\left(\frac{-A_c^2}{2\langle w^2\rangle}\right), \quad \mathbb{P}(E > \varepsilon_c) \equiv \mathbb{P}_\varepsilon = \exp\left(\frac{-\varepsilon_c^2}{2\langle\varepsilon^2\rangle}\right).$$

   Therefore if ε_c is an estimate for the breaking strain of ice, the probability of no breaking occurring is $\mathbb{P}_{\mathrm{nb}} \equiv (1-\mathbb{P}_\varepsilon)^{N_{\mathrm{W}}}$. We then suppose that breaking occurs if $1 - \mathbb{P}_{\mathrm{nb}} > \mathbb{P}_{\mathrm{c}}$, where we choose $\mathbb{P}_{\mathrm{c}} = 0.5$, since we have only the two options of breaking or not-breaking. In terms of E_s, this criterion is

$$E_s > E_c = \varepsilon_c \sqrt{-2/\log\left(1 - (1-\mathbb{P}_{\mathrm{c}})^{1/N_{\mathrm{W}}}\right)}. \tag{3}$$

4. *Update the floe size distribution.* Let $T_{\mathrm{W}} = \Delta t/N_{\mathrm{W}}$ be the average time between waves during our time interval. This lets us estimate a typical wavelength λ_{ij}. If breaking occurs, we reduce the maximum possible floe size from D_{ij}^{M} to $\lambda_{ij}/2$ (although we have a lower limit of 20 m below which D_{ij}^{M} cannot fall). We can now calculate $\langle D_{ij}\rangle$ and move on to the next time step.

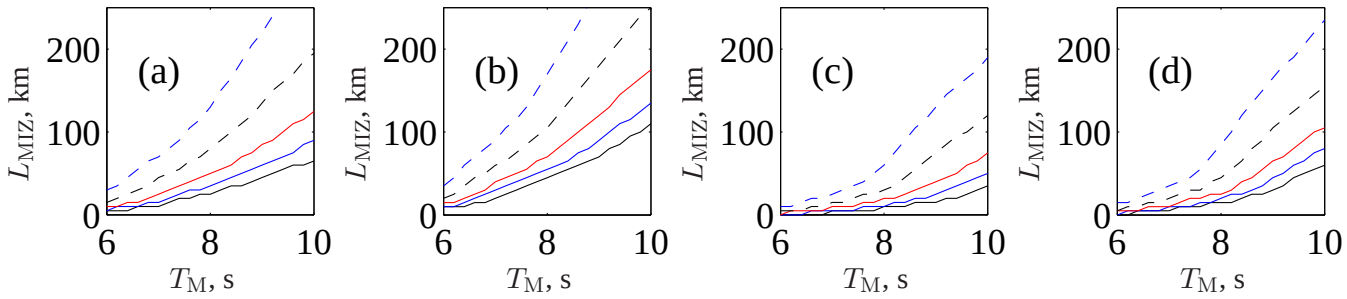

Figure 2: The effect of the value of the endurance breaking strain ε_c and the significant wave height H_s on L_{MIZ}. The time step is set to 260 s and wave speed is set to $\Delta x/\Delta t$ for all wave frequencies (so AAS 1 and 2 are equivalent). In (a-b) $h = 2$ m, while in (c-d) $h = 3$ m, and in (a, c) $H_s = 1.5$ m, while in (b, d) $H_s = 2.5$ m. In all plots the concentration is uniformly 0.75, while $\varepsilon_c = 5.5 \times 10^{-5}\beta$, where β takes the values of 0.2 (dashed blue curves), 0.5 (dashed black), 1 (red), 1.5 (solid blue) and 2 (solid black).

One-dimensional numerical results

In a one-dimensional model, there is only one wave direction, so we leave out the G factor in (2). The advection and attenuation is also much simpler so we can easily try out more complicated schemes. The first combination of steps 1 and 2 we shall call Advection-Attenuation Scheme 1 (AAS 1), in which $\tilde{S}$ is given by the simple scheme

$$\tilde{S}(\omega, x_i, t_n) = S(\omega, x_i, t_{n-1}) + a_i(\omega)\frac{\Delta t}{\Delta x}\big(S(\omega, x_{i-1}, t_{n-1}) - S(\omega, x_i, t_{n-1})\big). \tag{4}$$

In our simulations we use $\Delta x = 5$ km. The first few left hand grid cells contain open water, with the left-most one containing a Bretschneider wave spectrum that travels right. (This cell is topped up with new waves every time step.) Each cell has specified constant thickness and concentration, and D_i^{M} is initially set to a large value. The width of the MIZ, L_{MIZ}, is defined as the length of the region in which breaking has occurred.

The second combination, labelled AAS 2, puts different frequencies on different time steps to make the advection more efficient. (Essentially we set the time step in equation (4) to $\Delta x/a_i(\omega)$; this requires us to interpolate in time to perform breaking, which occurs at a global time step.) In addition, the attenuation process is modified so that a given wave packet is not overly attenuated. The spurious attenuation comes from the discretisation—a packet can arrive in a grid cell but not completely leave it in the space of one time step. Since $\langle D_i \rangle$ is constant over each grid cell, if such a packet arrives and causes breaking, the broken ice is effectively moved from behind it to in front of it, thus causing it to experience additional attenuation before it leaves the cell.

Figure 1 shows the importance of using a reliable AAS in the WIM. Figures (a) and (c) show the results for L_{MIZ} when waves of different frequencies move at the same speed. Different values for this speed are investigated in figures (a) and (c), and it is found that under AAS 2, it has little effect on the results (as it shouldn't). In contrast, when using AAS 1, reducing the speed from $\Delta x/\Delta t$ can cause L_{MIZ} to be underestimated by a factor of up to 3. Figures (b) and (d) show the effect of including dispersion—here the wave speeds are scaled, but they disperse by the same amount as waves in open water do. The dispersion causes L_{MIZ} to drop slightly and there is more fine structure in the curves. Again, the results from AAS 2 are very robust, and the MIZ is about twice as wide as under AAS 1. The AAS 2 curves show some fine structure that seems robust under changes to $\boldsymbol{\mathcal{C}}$ (or equivalently, to the maximum wave speed). These can be attributed to E_s being closer to its threshold E_c, and are thus more sensitive to the balance between increased attenuation and lower strain values as wave period increases. As in the same-speed results, AAS 2 generally produces much a wider MIZ than AAS1.

Figure 2 shows the sensitivity of the results to the values of the significant wave height H_s and the breaking strain ε_c. Comparing (a) and (c) with (b) and (d) we see that, as expected, increasing H_s increases L_{MIZ}. Similarly, decreasing ε_c increases L_{MIZ}. The effect is more marked for the two lower values (dashed curves), but there is still clear variation among the three higher values (solid curves), showing that good estimates for the ice properties are important. By referring to (3), we can see that changing ε_c also includes the effects of changing Δt (through N_{W}) and $\mathbb{P}_{\mathrm{c}}$. However, changing these latter two (within reason) only produces variations in E_c of about 5–10%, so we do not expect them to have a significant impact.

Both figures 1 and 2 also show the effect of increasing the thickness from 2 m to 3 m. This has the effect of reducing L_{MIZ} by about $\frac{2}{3}$, mainly by increasing the attenuation.

Preliminary results for the two-dimensional model

Figure 3 shows some preliminary two-dimensional results. They were computed on a CRAY XT4 using 51 parallel 2.3 GHz CPUs with 1 GB memory per CPU. (Not all of this is needed for the WIM—a significant portion of these resources runs the ocean/ice model that the WIM is coupled to.) We have an initial wave forcing that is prescribed as shown in (d), and it is advected into the ice using a WENO scheme and in 10 directions with a resolution of 21.2°. In all figures, mid-grey areas represent land, while open ocean is coloured blue in (a-c) as D_{ij}^{M} is set to 0 m there. All the waves travel at the same speed $a = 0.73 \times \min\{\Delta x\}/\Delta t$. Unlike in the one-dimensional simulations, the waves are not topped up every time step. A sophisticated AAS like AAS 2 is more difficult to implement in two-dimensions, so for now we simply wait one time step

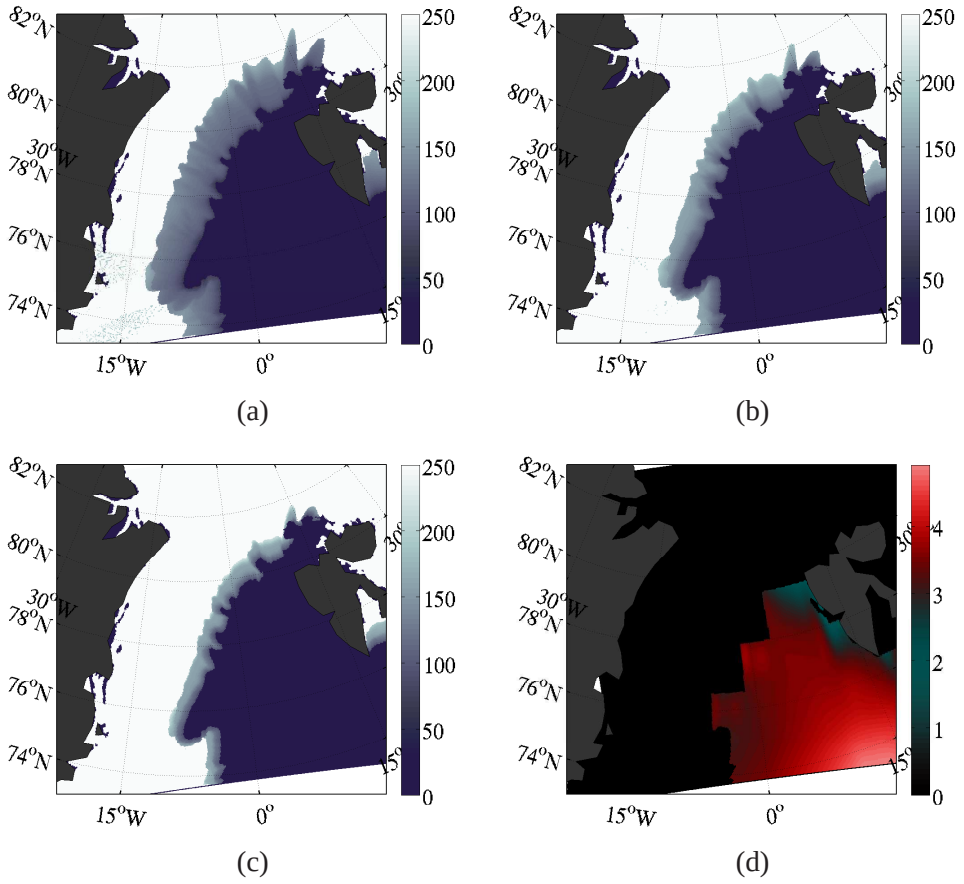

Figure 3: Preliminary results for the maximum floe size D_{ij}^{M} (in metres), when the ice concentration is a constant 0.8, and the thickness is a constant of (a) 2 m, (b) 3 m or (c) 4 m. The ice extent comes from the HYCOM model predictions for 2 January 2000, and the wave forcing for the same day comes from the WAM model. The significant wave height H_s (also in metres) is shown in (d), the mean wave direction is 187°, and 10 wave directions between $-9°$ and 221° are included with a resolution of 21.2°. The mean peak period is 10.5 s.

before updating the attenuation coefficient in a cell where breaking occurs. For $\boldsymbol{\mathcal{C}} = 0.73$, this should let waves that cause breaking in a grid cell escape without being overly attenuated. Also, since dispersion is not included, it is probable that our results slightly overestimate the impact of waves on the ice cover (as predicted by the current theory).

The figure shows the variation of the results with ice thickness. Using moored upward looking sonar data, *Vinje et al.* (1998) constructed time series of ice thickness in Fram Strait by measuring ice draft every four minutes, i.e. a nominal sampling interval of 30 m. These authors found that the modal ice thickness has a maximum of 3.15 m in May and a minimum in September of 2.43 m, an annual variation range of 0.72 m. This compares well with early model results, comprehensive drillings, and most of the submarine observations during the 2–3 decades prior to the *Vinje et al.* dataset, indicating no significant long-term ice thickness change up to 1998. (This date is close to our HYCOM simulations of 2 January 2000, so it is not unreasonable to take thickness estimates between 2 and 3 m as representative of Fram Strait sea ice at the time.) In Figure 3 the MIZ for the 2-m-thick ice is probably the most realistic-looking one, so it is likely that we are underestimating the MIZ width by about a factor of 2 . It is unclear at this time precisely how this could be improved significantly but, given the difficulty of what we are attempting, the authors are pleased with the results so far.

Acknowledgements

The WIFAR project is funded by the Research Council of Norway and Total E&P Norge. The one-dimensional results are sampled from a longer manuscript (in preparation) with additional co-authors Laurent Bertino (NERSC) and Dany Dumont (Institut des sciences de la mer de Rimouski).

References

Bennetts L. G. and Squire V. A., 2012. On the calculation of an attenuation coefficient for transects of ice-covered ocean, *Proc. Roy. Soc. A*, 468 (2137), 136–162

Dumont D., Kohout A. and Bertino L., 2011. A wave-based model for the marginal ice zone including a floe breaking parameterization, *J. Geophys. Res.*, 116 (C04001)

Squire, V., and S. C. Moore (1980), Direct measurement of the attentuation of ocean waves by pack ice, *Nature*, *283*(5745), 365 – 368.

Vinje T, Nordlund N. and Kvambekk A, 1998. Monitoring ice thickness in Fram Strait, *J. Geophys. Res.*, 113 (C5), 10437 – 10449

World Meteorological Organization (1998), *Guide to Wave Forecasting and Analysis*, WMO No. 702, 2 ed.